Electronic version of an article published as International Journal of Bifurcation and Chaos Vol. 10, No. 8, 2000, 1917-1931,
DOI: 10.1142/S0218127400001183 © World Scientific Publishing Company, https://www.worldscientific.com/worldscinet/ijbc

Bifurcation Analysis of Chen's Equation

Tetsushi Ueta and Guanrong Chen

Department of Information Science and Intelligent Systems
Tokushima University, Tokushima, 770-8506 Japan
tetsushi@is.tokushima-u.ac.jp
Department of Electrical and Computer Engineering
University of Houston, Houston, Texas, 77204 USA
gchen@uh.edu

Abstract

Anti-control of chaos by means of making a non-chaotic system chaotic has led to the discovery of some new chaotic systems, particularly the continuous-time three-dimensional autonomous Chen's equation with only two quadratic terms. This paper further investigates some basic dynamical properties and various bifurcations of Chen's equation, thereby revealing its different features from some other chaotic models such as the Lorenz system.

1 Introduction

Over the last two decades, chaos in engineering systems such as nonlinear circuits has gradually moved from being simply a curious phenomenon to one with practical significance and applications. Chaos has been found to be useful or have great potential in many disciplines such as in thorough liquid mixing with low power consumption, high-performance circuit design for telecommunication, collapse prevention of power systems, biomedical engineering applications to the human brain and heart, to name just a few [Chen 1999; Chen & Dong 1998].

Creating chaos, therefore, becomes a key issue in such applications where chaos is important and useful. Given a system or process, which may be linear or nonlinear but is originally non-chaotic or even stable, the question of whether or not one can generate chaos (and, if so, how) by means of designing a simple and implementable controller (e.g., a parameter tuner or a state feedback controller) is known as *anti-control of chaos* or *chaotification*. This problem is theoretically attractive and yet technically very challenging, as can be imagined from the complicated behavior of chaos and its association with various bifurcations.

Nevertheless, tremendous efforts have been devoted to trying to achieve this goal not only via computer simulations for the task but also by developing complete and rigorous mathematical theories to support the task. In this endeavor, anti-control of discrete chaos has seen success whereby chaos is generated in an "arbitrarily given" system via a simple nonlinear state feedback controller – more precisely, for any given finite-dimensional discrete-time system with a bounded Jacobian, chaotification can be achieved by a linear state feedback plus a modulo operation [Chen & Lai, 1998] or a piecewise-linear sawtooth function [Wang & Chen, 1999]. Moreover, it was rigorously justified in these papers that the generated chaos satisfied the mathematical definition of chaos.

Moving forward from the discreate-time systems to the continuous-time setting, a simple linear partial state-feedback controller was found to be able to derive the Lorenz system, currently not in the chaotic region, to be chaotic. In fact, it led to the discovery of a new chaotic system, which is competitive with the Lorenz system in the structure (it is a three-dimensional autonomous equation with only two quadratic terms), topologically not equivalent (there does not exist a homeormophism that can take one system to the other), and yet has even more complex dynamical behavior than the Lorenz system [Chen & Ueta, 1999]. This paper is devoted to a more detailed analysis of this new chaotic system — the chaotic Chen's equation (see also [Yu & Xia, 2000].

2 Anti-Control of the Lorenz Equation

In this section, we focus on the creation of chaos with anti-control techniques. We try to destabilize some existing stable equilibria of non-chaotic system by using state feedback. This method not always yields chaotic situation, however; it may work out if the equilibria have hyperbolic structures in a globally bounded system.

Consider the controlled Lorenz equation:

$$\begin{aligned} \frac{dx}{dt} &= a(y-x) \\ \frac{dy}{dt} &= cx - xz - y + u \\ \frac{dz}{dt} &= xy - bz \end{aligned} \tag{1}$$

where a, b, c are constants, currently not in the range of chaos, and u is a linear feedback controller of the form

$$u = k_1 x + k_2 y + k_3 z\,, \tag{2}$$

in which k_1, k_2, k_3 are constant gains to be determined. The controlled system Jacobian, evaluated at (x^*, y^*, z^*), is given by

$$J_{(x^*,y^*,z^*)} = \begin{bmatrix} -a & a & 0 \\ c + k_1 - z^* & k_2 - 1 & k_3 - x^* \\ y^* & x^* & -b \end{bmatrix} \tag{3}$$

To find the equilibria of the controlled Lorenz system (1)–(2), let

$$\begin{aligned} a(y-x) &= 0 \\ (c+k_1)x - xz + (k_2-1)y + k_3 z &= 0 \\ xy - bz &= 0 \end{aligned} \tag{4}$$

Obviously, $(0, 0, 0)$ is a trivial equilibrium.

To find non-zero equilibria, observe that the first equation of (4) yields immediately $x = y$, so that the third one gives $z = \frac{1}{b}\, x^2$. Therefore, the second equation of (4) leads to

$$x = y = \frac{1}{2}\, k_3 \pm \frac{1}{2}\, \sqrt{k_3^2 + 4b(c + k_1 + k_2 - 1)} \tag{5}$$

It can be easily seen from the Jacobian (3) that if this Jacobian is evaluated at the zero equilibrium, $(x^*, y^*, z^*) = (0, 0, 0)$, then k_3 does not contribute to its eigenvalues, which means k_3 does not contribute to the system Lyapunov exponents. Therefore, we may choose $k_3 = 0$ for simplicity. To further determine k_1 and k_2 for possible chaotic behavior of the system (1) under anti-control (2), we turn to the system Jacobian (3) evaluated at the two non-zero equilibria (5). To have chaotic behavior, these equilibria cannot be stable, or in other words, we have to have at least one unstable eigenvalue at each of these two equilibria. The Routh test reveals a simple possible choice, among several others, of

$$k_1 = -\,a \qquad \text{and} \qquad k_2 = 1 + c$$

Luckily, computer simulations have shown that these gains indeed yield a successful anti-controller:

$$u = -\,a\,x + (1 + c)\,y \tag{6}$$

which leads the controlled, currently non-chaotic Lorenz equation (1)–(2) to the following chaotic Chen's equation:

$$\begin{aligned} \frac{dx}{dt} &= a(y-x) \\ \frac{dy}{dt} &= (c-a)x - xz + cy \\ \frac{dz}{dt} &= xy - bz \end{aligned} \tag{7}$$

Figure 1(a) shows a phase portrait of the non-chaotic Lorenz equation with $a = 35$, $b = 8/3$, $c = 28$, in which an orbit started from an arbitrary initial point is attracted into a sink. On the contrary, we see in Fig. 1 (b) a chaotic attractor in the anti-controlled system (7) with the same set of parameter values. Besides, as stated below, boundedness of the anti-controlled system is guaranteed. These results suggest that the anti-controlling action is effective to create chaotic behavior in some cases like this one.

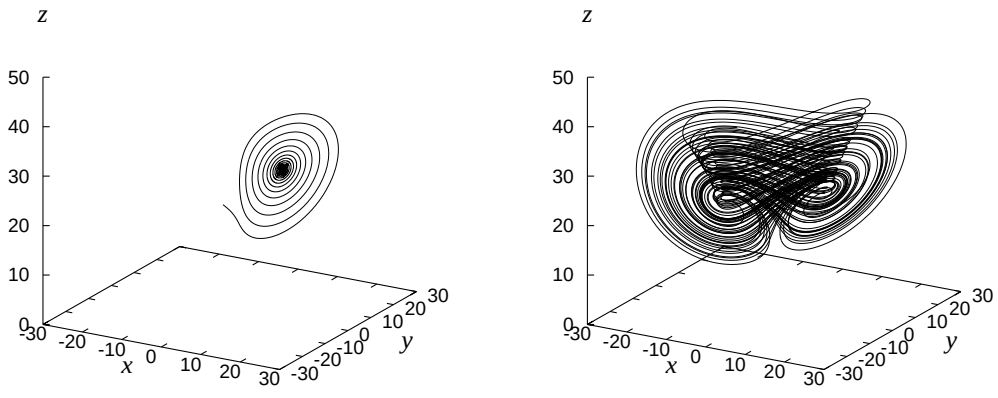

(a) (b)

Figure 1: Phase portraits. (a): Uncontrolled Lorenz system, (b): Anti-controlled Lorenz system. $a = 35$, $b = 8/3$, $c = 28$. $(x_0, y_0, z_0) = (-3, 2, 20)$.

3 Dynamical Properties of Chen's Equation

3.1 Some Mathematical Properties

This section discusses some basic dynamical properties of Chen's equation (7). This system has the same complexity as the Lorenz equation — they are both three-dimensional autonomous with only two quadratic terms. However, it is topologically not equivalent to the Lorenz equation. This can be rigorously proved by showing that a homeomorphism of the form

$$\begin{cases} x_C = \xi(x_L, y_L, z_L) \\ y_C = \eta(x_L, y_L, z_L) \\ z_C = \zeta(x_L, y_L, z_L) \end{cases} \tag{8}$$

does not exist, where (x_L, y_L, z_L) and (x_C, y_C, z_C) are the variables of the Lorenz and Chen equations, respectively. The proof can be carried out by taking a time derivative on (8) and then performing some straightforward but tedious algebra, which leads to a system of algebraic equations without solutions.

It is easy to see that this equation has a trivial property of symmetry: the equation is invariant under the following transformation:

$$(x, y, z) \to (-x, -y, z) \tag{9}$$

Then, let us rewrite Eq. (7) in the following vector form:

$$\frac{d\boldsymbol{x}}{dt} = \boldsymbol{f}(\boldsymbol{x}) \tag{10}$$

where $\boldsymbol{x} = (x, y, z) \in \boldsymbol{R}^3$, and $\boldsymbol{f}(\boldsymbol{x})$ is the right-hand side of Eq. (7). The transformation (9) can now be denoted as

$$P\colon \boldsymbol{R}^3 \to \boldsymbol{R}^3; \qquad \boldsymbol{x} \mapsto P\boldsymbol{x}, \qquad P = \begin{pmatrix} 0 & -1 & 0 \\ -1 & 0 & 0 \\ 0 & 0 & 1 \end{pmatrix} \tag{11}$$

which satisfies

$$\boldsymbol{f}(P\boldsymbol{x}) = P\boldsymbol{f}(\boldsymbol{x}) \tag{12}$$

The dynamics of the system is affected by this symmetry. For example, in the projection of its orbits onto the phase plane, variable x and y are symmetric with respect to the origin. Besides, this hints that pitchfork bifurcation for equilibria and periodic solutions are possible.

Let us examine the stability of Chen's system. It is easy to verify that the system is globally, uniformly and asymptotically stable about its zero equilibrium if $c < 0 < a$. This can be checked by using the Lyapunov function

$$V(x, y, z) = \frac{a - c}{2a}\, x^2 + y^2 + z^2$$

which gives

$$\dot{V} = -(a - c)x^2 + c\, y^2 - bz^2 < 0$$

Next, let us consider a volume in a certain domain D_0 of the state space. Notice that

$$\operatorname{div} \boldsymbol{f}(\boldsymbol{x}) = -a - b + c. \tag{13}$$

We always use a set of parameters satisfying $-a - b + c < 0$, such as $(a, b, c) = (35, 3, 28)$ [Chen & Ueta, 1999]. This means that the dynamical system (7) is guaranteed to be dissipative, so the volume of any attractor of the system must be zero. The orbit flows into a certain bounded region as $t \to \infty$.

3.2 Bifurcations of Equilibria

The dynamical system described by Eq. (7) has three equilibria if $(2c - a)b > 0$:

- $O = (0, 0, 0)$
- $C^+ = \left(\sqrt{(2c - a)b},\ \sqrt{(2c - a)b},\ 2c - a \right)$
- $C^- = \left(-\sqrt{(2c - a)b},\ -\sqrt{(2c - a)b},\ 2c - a \right)$

By considering a Jacobian matrix for one of these equilibria and calculating their eigenvalues, we can investigate the stability of each equilibrium based on the roots of the system characteristic equation.

Here, we first observe some bifurcations of the equilibria existing in Eq. (7). We gradually change the values of a. When $a > a_n$, the origin O is the only equilibrium and it is a sink, where

$$a_n = \frac{(3 + 2\sqrt{3})c}{3} \tag{14}$$

is the parameter value at which the sink changes to a node. Then, a pitchfork bifurcation for O emerges at the value of

$$a_p = 2c \tag{15}$$

At this moment, O changes to a one-dimensionally unstable saddle and, at the same time, two symmetric sinks are generated, so we have three equilibria when $a < a_p$. The parameter a_p is also the tangent/saddle-node bifurcation value for both C^+ and C^-. Note that these bifurcations do not depend on parameter b.

Hopf bifurcations emerges from these sinks, at the value of

$$a_h = \frac{3c + \sqrt{-8bc + 17c^2}}{4} \tag{16}$$

where the complex conjugate eigenvalues are $\mu = \pm i\sqrt{bc}$. When $a_h < a < a_p$, C^+ and C^- are both stable sinks. At $a = a_h$, however, they change to two two-dimensional unstable saddles, and two isolated limit cycles are generated around them, respectively. These simulation results are combined into the figures shown in the next section.

3.3 Bifurcations of Periodic Solutions

In this section, we fix $c = 28$ and investigate the behavior of system limit cycles.

We use the Poincaré mapping method to investigate the properties of periodic solutions of Eq. (7). We take an appropriate local plane as the Poincaré section, for instance, $y = \sqrt{(2c - a)b}$ or $y = 0$, and then calculate the bifurcation parameter values by using the Poincaré map and its derivatives.

There are three kinds of local bifurcations for periodic solutions in this system:

- tangent bifurcation: T
- pitchfork (symmetry-breaking) bifurcation: Pf
- period-doubling bifurcation: Pd

The parameter values that generate these bifurcations are calculated by simultaneously solving the fixed point of the Poincaré map and the system characteristic equation.

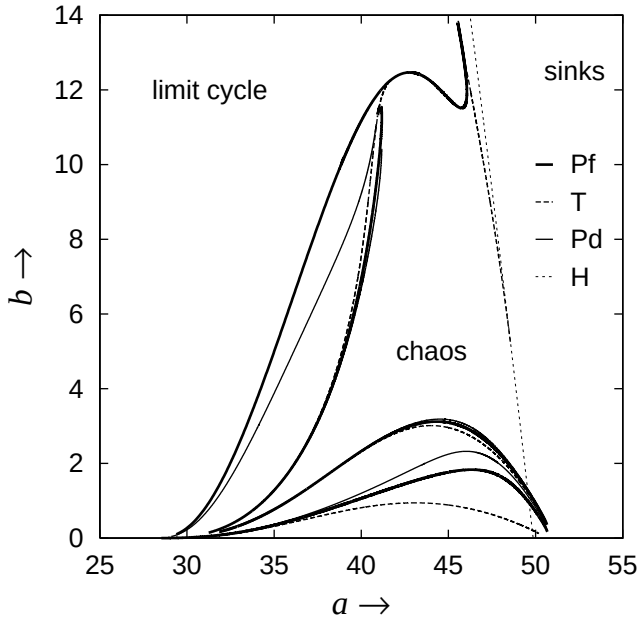

Figure 2: Bifurcation diagram of Eq. (7). $c = 28$.

Figure 2 shows a bifurcation diagram in the a–b plane for periodic solutions. In this figure, roughly speaking, there exist three divisions in the plane. Each region has stable attractors, i.e., sinks (C^+ and C^-), chaos, and limit cycles. Many islands (windows) giving periodic solutions are embedded in the chaotic region. Each island is basically composed of a set of bifurcation curves (T, Pf, Pd), as illustrated by Fig. 3.

Figure 4 shows an enlargement of Fig. 2. Let us first observe the responses of the system when the parameter b changes gradually from the lower part to the upper part along the line $\overline{\mathrm{ae}}$. The periodic solution, shown in Fig.5 (a), is generated by the tangent bifurcation T via intermittent chaos. This solution is divided into two stable limit cycles after crossing the pitchfork bifurcation Pf, see Fig 5 (b). They form the Lorenz-linkage [Jackson, 1991]. Let $\boldsymbol{x}(t) = \boldsymbol{\varphi}(t, \boldsymbol{x}_0)$ be a solution of this system with initial condition $\boldsymbol{x}_0 = \boldsymbol{\varphi}(0, \boldsymbol{x}_0)$. Let $\boldsymbol{\varphi}_1(t)$ and $\boldsymbol{\varphi}_2(t)$ be the limit cycles generated by Pf. The relationship between these two cycles is as follows:

$$\boldsymbol{\varphi}_1(t, \boldsymbol{x}_0) = P\boldsymbol{\varphi}_2(t, P\boldsymbol{x}_0), \qquad \boldsymbol{\varphi}_2(t, \boldsymbol{x}_0) = P\boldsymbol{\varphi}_1(t, P\boldsymbol{x}_0) \tag{17}$$

Each of them is bifurcated to period-2 solutions when crossing the period-doubling bifurcation Pd_1, see Fig. 5 (c). When these solutions meet Pd_2, we have period-4 solutions. Via period-doubling cascade, finally it develops into a chaotic attractor as shown in Fig. 5 (d). Thus, there exist two isolated chaotic attractors in the state space. It can be observed by further

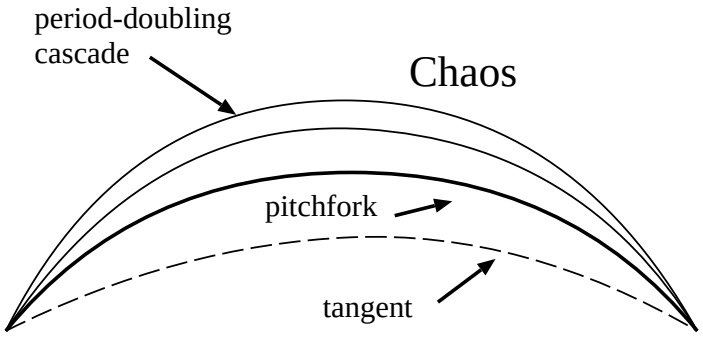

Figure 3: Typical structure of the periodic-locking region.

changing the value of b that these isolated chaotic attractors are merged. The attractor looks like the Lorenz attractor, see Fig. 5 (e), namely, there are two spirals and the orbit tend asymptotically to some two-dimensional surface in the state space.

On the other hand, by changing parameter a along the line $\overline{\text{fk}}$, Figs. 5 (f)–(k) are obtained, which show the corresponding phase portraits. We can see the same bifurcation scenario. However, the chaotic attractor shown in Fig. 5 (k) is somewhat different from a Lorenz-type attractor by means of its spiral shape over the two screws, which does not have the tendency to move to any two-dimensional surface. We further discuss this attractor in Sec.3.4.

Figure 6 shows bifurcation curves that form another island. Figures 7 (a)–(d) are phase portraits observed on the parameter sets a–d indicated in Fig. 6. Also, the same bifurcation scenario can be observed.

Figure 10 is also an enlargement of the upper part of Fig. 2, showing regions sectioned by bifurcation curves. In each region, there exists at least one topologically different stable attractor against another region. The tangent bifurcation curve T for a limit cycle is coalesced by the pitchfork bifurcation curve Pf. Thus, two periodic orbit generated by Pf is immediately disappeared by T at the boundary of (A) and (F). In region (F), we have a chaotic attractor as shown in Fig. 8. This attractor is probably related to a kind of homoclinic orbits about O, since some parts of the orbit are tangent to the plane including unstable manifolds of O, as can be seen from Fig. 8 (a)–(d). This chaotic orbit changes its shape to be Lorenz-like, when the parameter is changed toward inside of region (F). This can be seen from Fig. 11. Further investigation of this orbit is very interesting but time-consuming, which will be summarized and presented in a future article. As the parameter set is changed from region (B) toward region (C), the limit cycle meets the period-doubling cascade diagram started from Pd. In region (C), there also exist chaotic solutions.

The island composed of regions (D) and (E) showing periodic motions connects to region (B). Figures 9 show the corresponding Lyapunov exponents along $b = 11$ from (A) to (F). From these exponents, it is seen that there exists a very narrow area exhibiting chaos between (C) and (D).

In Fig. 10, the curve H shows Hopf bifurcation for $C^{\pm}$ described by Eq. (16). There is no stable periodic solution in region (I), and there exist two stable limit cycles in region (G). In fact, there also exist two unstable (saddle-type) limit cycles in this region. Figure 12 shows these limit cycles and the unstable equilibria. These two cycles disappear when reaching the tangent bifurcation T. After this bifurcation, one can see a chaotic attractor as shown in Fig. 11. Note that this chaotic attractor can survive in regin (I); in other words, coexistence of stable equilibria and chaotic attractor occurs in region (I).

3.4 Dynamical Structure of the Chaotic Attractor

In this section, we focus our attention on the dynamical structure of the strange attractor shown in Figure 5 (k), where $(a, b, c) = (35, 3, 28)$. Figure 13 (a)–(c) show the projections of the attractor onto the x-y, y-z, and x–z planes, respectively. The origin O is a one-dimensionally unstable saddle and its eigenvalues are -30.836, 23.836 and -3.0. $C^{\pm} = (\pm 3\sqrt{7}, \pm 3\sqrt{7}, 21)$ are two-dimensionally unstable and their corresponding eigenvalues are -18.428 and $4.214 \pm i14.885$.

Figures 14(a)–(c) show Poincaré mapping on several sections. Several sheets of the attractors are visualized. In Fig. 14(d), it is clear that some sheets are folded.

Figure 15 shows the shapes of the stable manifolds for $C^{\pm}$. These one-dimensional manifolds wander over the chaotic attractor. Note that stability of these stable manifolds (negative eigenvalue) around $C^{\pm}$ is very strong.

Let us summarize how the attractor is formed. The orbit starting from an initial point whose values are sufficiently big must move to the $z > 0$ portion of equilibria because the instability of the unstable manifold of O is very strong and grows up

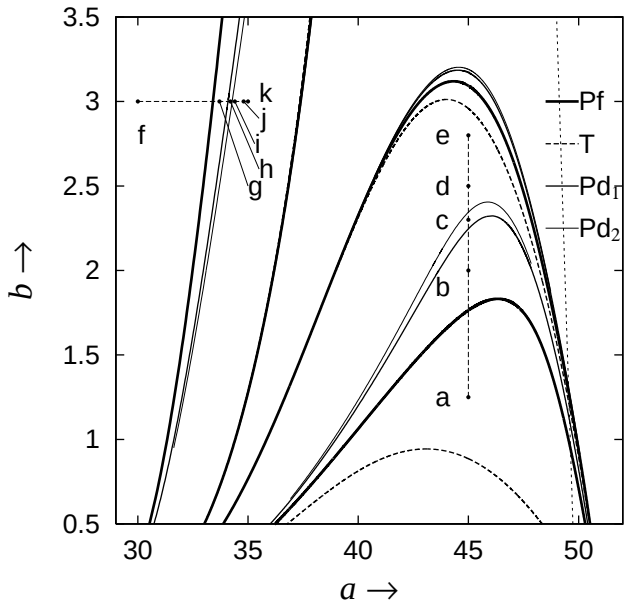

Figure 4: Enlargement of Fig. 2.

toward $z > 0$. Then the orbit draws elliptically in the x-y plane, decreasing the value z. It flows along the stable manifold of $C^{\pm}$, and takes a shape like a spiral in the y-z or x-z plane. After this, the orbit reached near $C^{\pm}$ goes away rapidly and scarcely turns on the 2-dimensionally unstable manifold of $C^{\pm}$ since the real part of the unstable eigenvalue is comparatively big. The orbit is then trapped into the unstable chaos as shown in Fig. 5 (i) for awhile. Finally, the orbit is lifted up along the unstable manifold of O. We can see that the stable manifolds of $C^{\pm}$ plays an important role in the generation of the strange attractor.

3.5 Comparison with the Lorenz Equation

The familiar Lorenz equation is given by

$$\begin{aligned} \frac{dx}{dt} &= a(y - x) \\ \frac{dy}{dt} &= cx - xz - y \\ \frac{dz}{dt} &= xy - bz \end{aligned} \tag{18}$$

Many research reports [Jackson, 1991; Argyris, 1994] mentioned its bifurcation structure in the c-b plane. We now show its bifurcation sets in the a-c plane in comparison with Chen's equation.

This system also has three equilibria: O, C^+, and C^-, and their topological properties are almost the same as that of Chen's equation (7). Figure 16 shows the bifurcation diagram of solutions of the Lorenz system (18). There exist islands of period-locking, which are the same as those shown in Fig. 2. The chaotic attractor, as shown in Fig. 17 (g), is widely observed in this parameter plane.

Hopf bifurcations at the equilibria, except for the origin, occurs at the value of

$$a_h = \frac{-3 - b - c + \sqrt{((3 + b - c)^2 - 4(1 + b)c)}}{2} \tag{19}$$

When $a < a_h$, the system orbit, starting from the neighborhood of C^+ or C^-, is trapped into the chaotic attractor. While if $a > a_h$, the chaotic attractor is eventually absorbed by C^+ or C^-. It is the well-known "crisis" phenomenon.

The stable manifolds of $C^{\pm}$ are very simple, as can be seen from Fig. 18. The mechanism of chaos is therefore completely different from Chen's strange attractor.

4 Conclusions

This paper has studied some basic dynamical properties and, in particular, various bifurcations of Chen's equation. It has shown that this equation has some essential different features from other typical chaotic models such as the Lorenz system. There are still some interesting issues about this new chaotic system, such as the properties of the homoclinic orbit in the sense of Shil'nikov, which deserve further investigation in the near future.

References

[1] Chen, G. (Ed.) [1999] *Controlling Chaos and Bifurcations in Engineering Systems*, Boca Raton, FL: CRC Press.

[2] Chen, G. & Dong, X. [1998] *From Chaos to Order: Methodologies, Perspectives and Applications*, Singapore: World Scientific Pub. Co.

[3] Chen, G. & Lai, D. [1998] "Feedback anticontrol of discrete chaos," *Int. J. of Bifur. Chaos*, **8**: 1585-1590.

[4] Chen, G. & Ueta, T. [1999] "Yet another chaotic attractor," *Int. J. of Bifur. Chaos*, **9**: 1465-1466.

[5] Jackson, E. A. [1991] *Perspectives of Nonlinear Dynamics*, Vol. 2, New York: Cambridge University Press.

[6] Argyris, J., Faust, G. & Haase, M. [1994] *An Exploration of Chaos*, Amsterdam: North-Holland.

[7] Wang, X. & Chen, G. [1999] "On feedback anticontrol of discrete chaos," *Int. J. of Bifur. Chaos*, **9**: 1435-1441.

[8] Yu, X. & Xia, H. [2000] "Detecting the periodic orbits of Chen's chaotic attractor," *Int. J. of Bifur. Chaos*, in press.

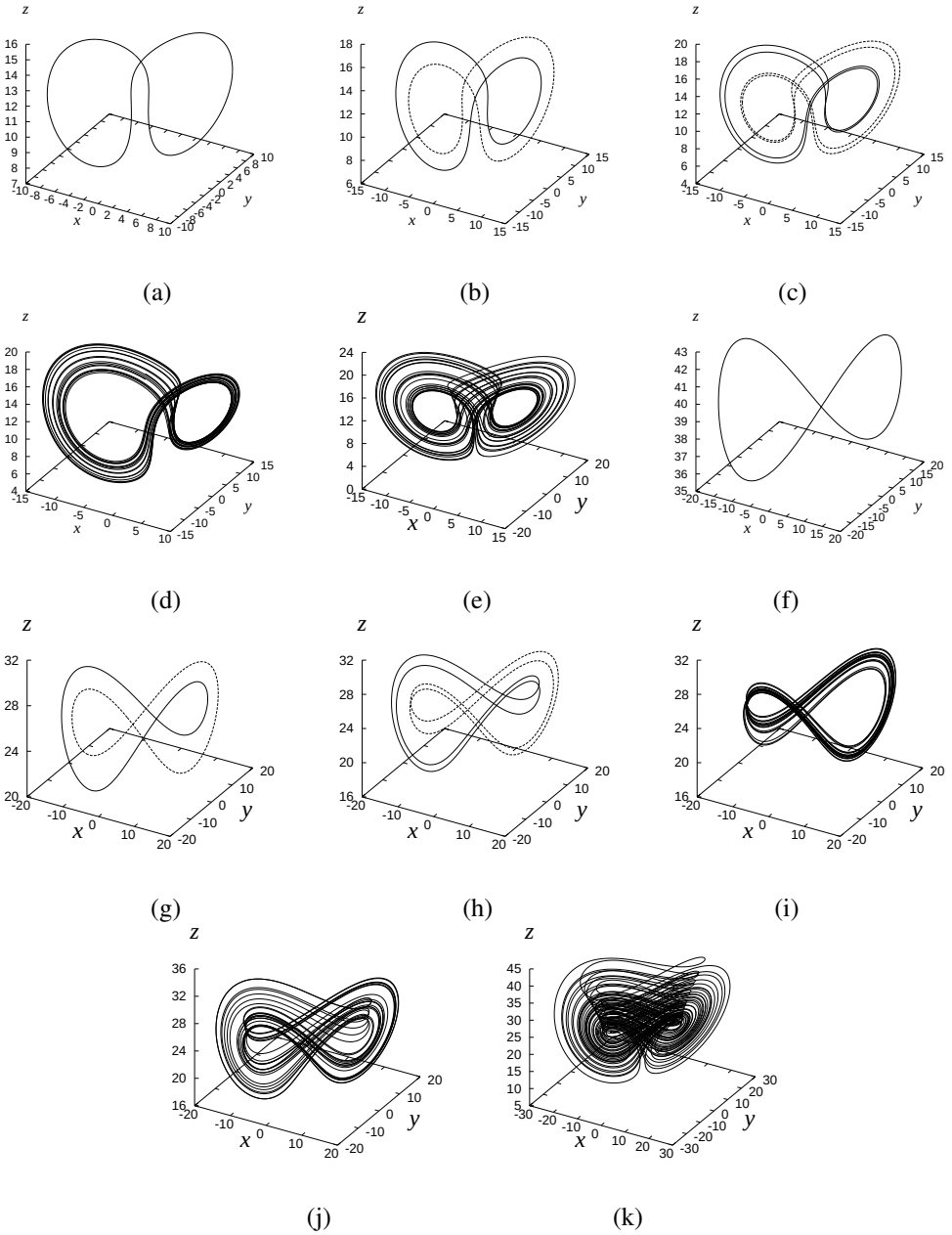

Figure 5: Phase portraits of stable attractors whose parameters are corresponding to Fig. 4 (a)–(k). (b), (c), (g) and (h) indicate two periodic solutions described by Eq. (17), simultaneously.

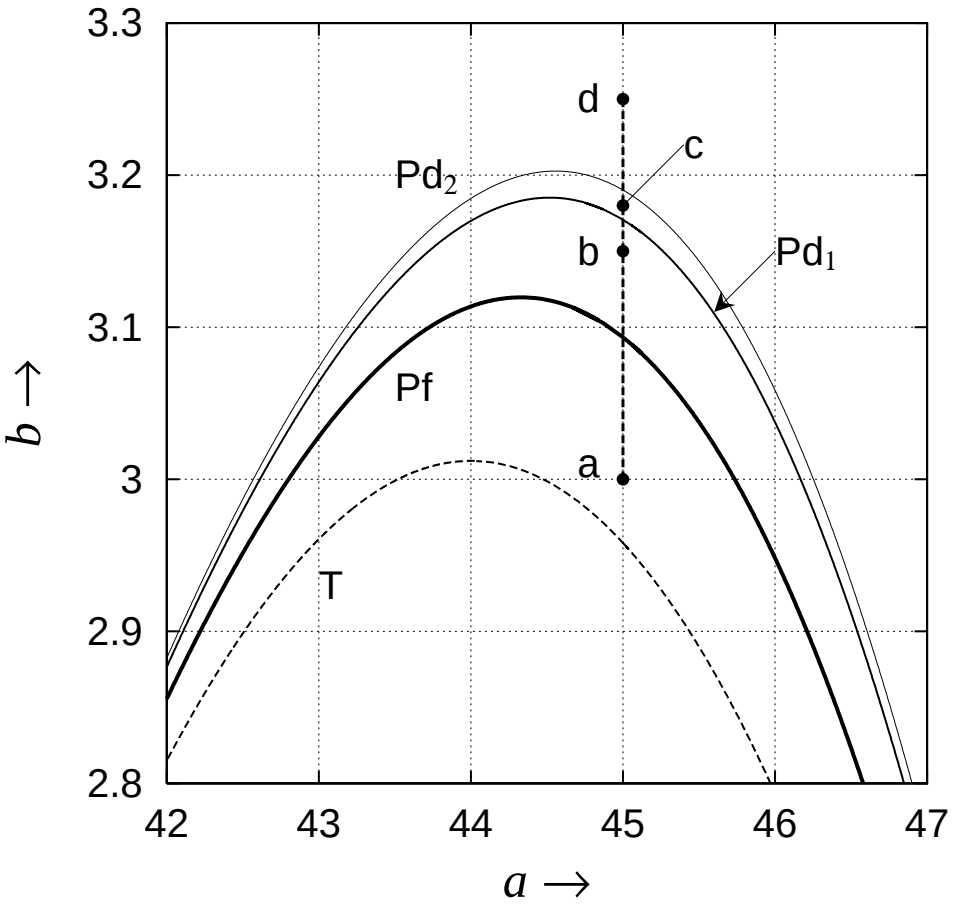

Figure 6: Enlargement of Fig. 4.

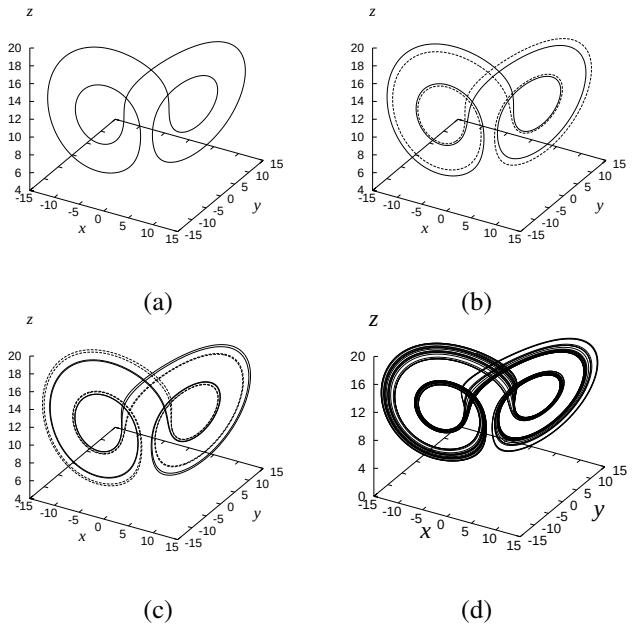

Figure 7: Phase portraits whose parameters are corresponding to Fig. 6 a–d.

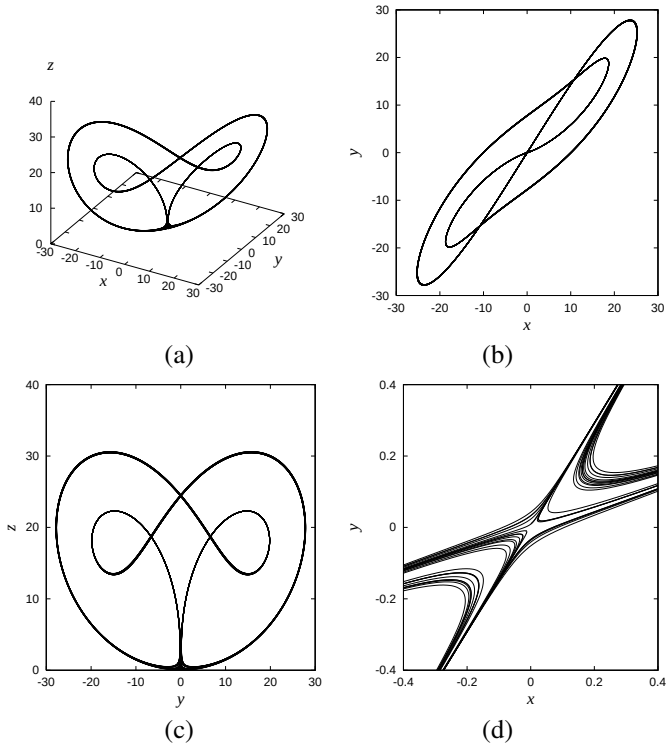

Figure 8: (a)–(c) A chaotic attractor observed near the boundaries of (A) and (F) in Fig. 10. (d): An enlargement around the origin. $a = 41.0181$, $b = 11.5$, $c = 28$.

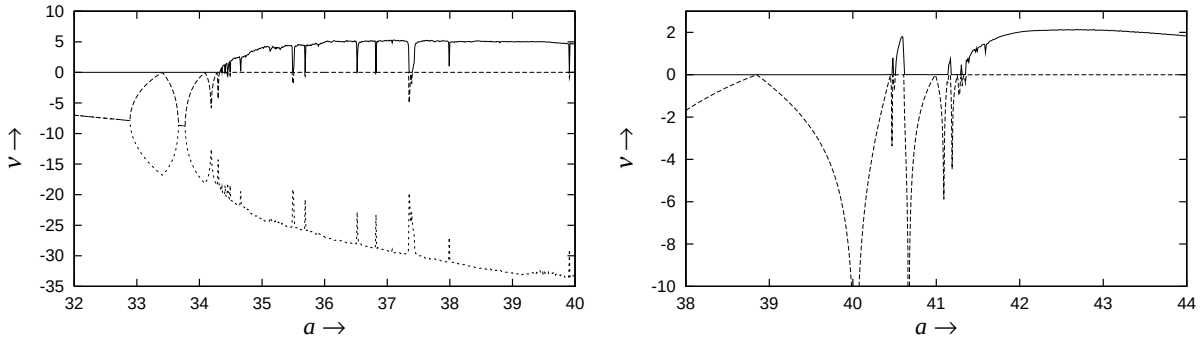

Figure 9: Lyapunov exponents. (a) $b = 3$, (b) $b = 11$, $c = 28$.

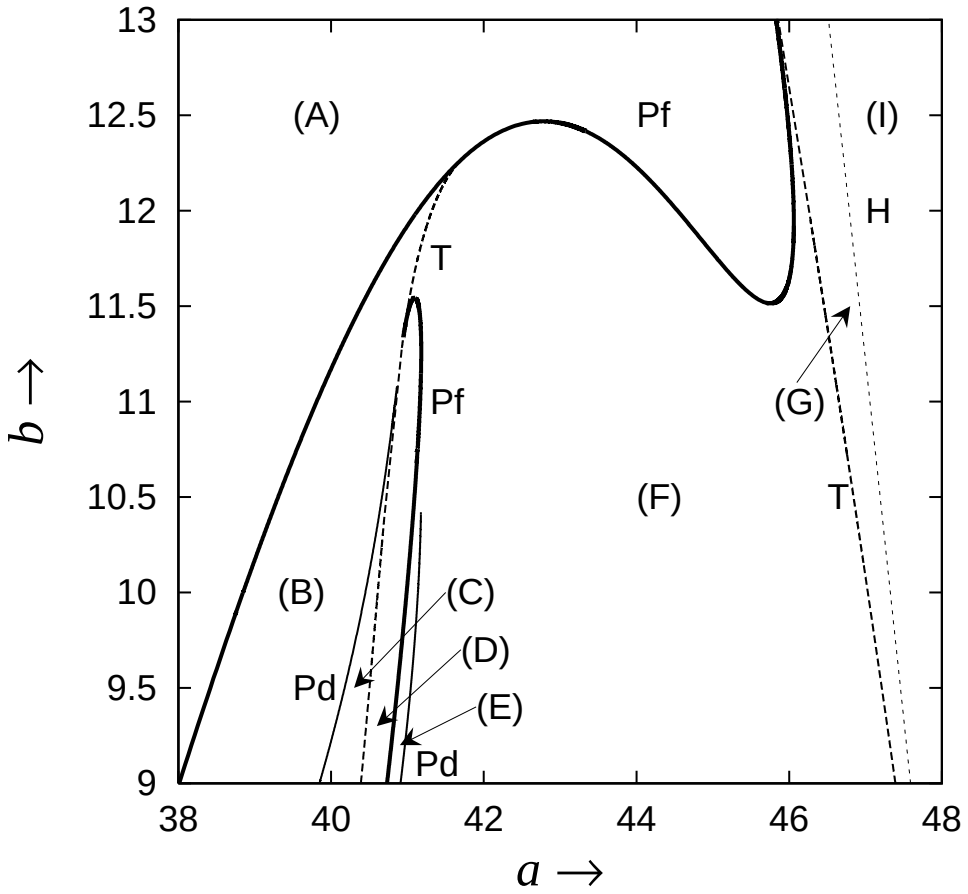

Figure 10: An enlargement of Fig. 2.

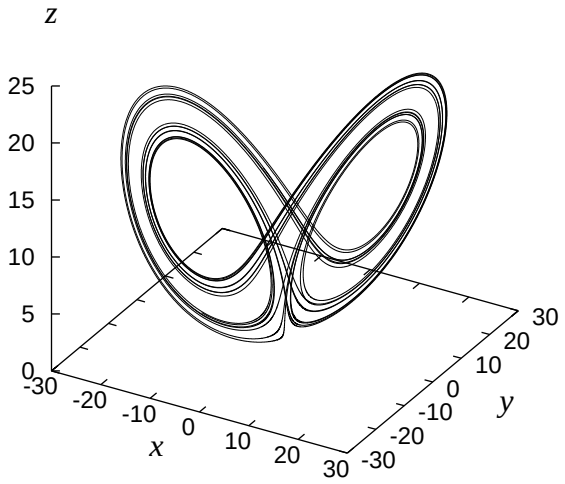

Figure 11: A typical chaotic attractor. $a = 44$, $b = 11$.

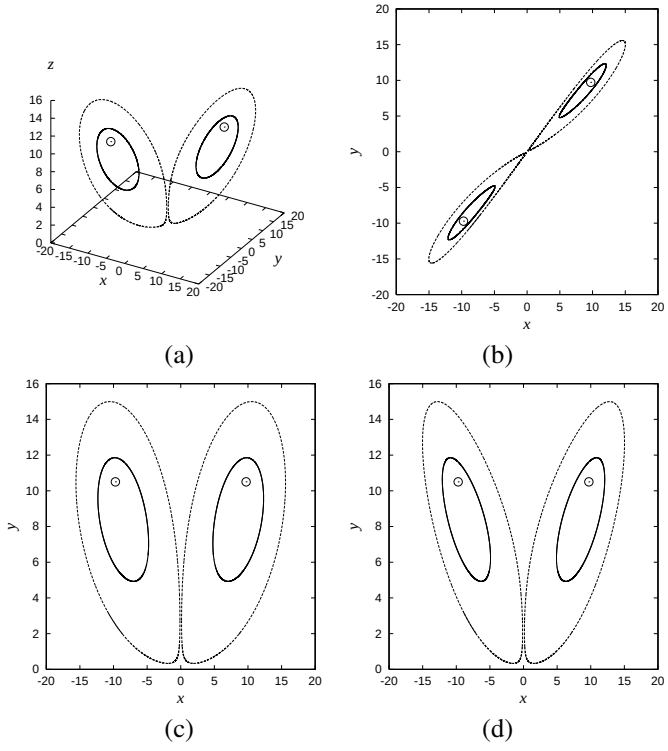

Figure 12: Attractors. dashed curve: unstable cycle; thin curve: stable cycle; small circle: unstable equilibrium. $a = 47.4979$, $b = 9$, $c = 28$.

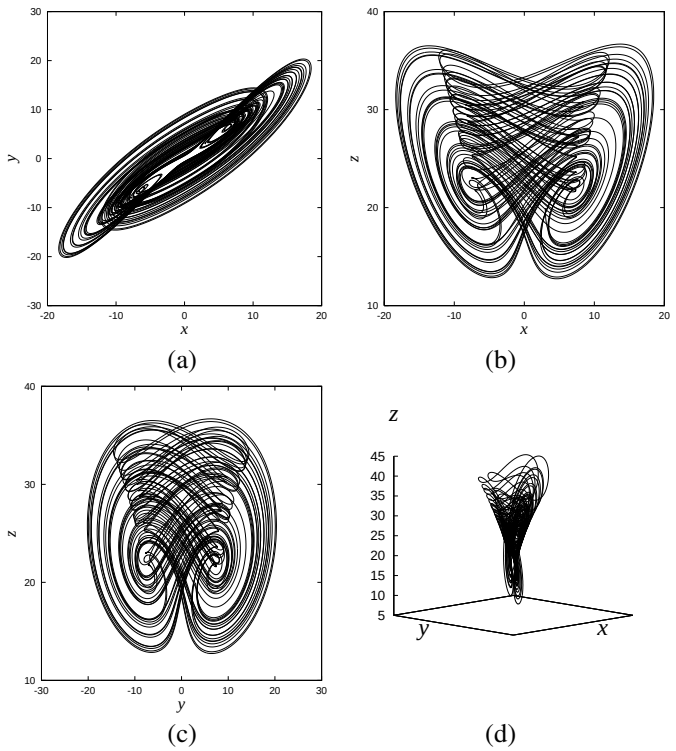

Figure 13: Various projections on the phase planes for the chaotic attractor shown in Fig. 5 (k). (a): x-y, (b): x-z, (c): y-z. (d): A perspective view (the view point is on $x = y$).

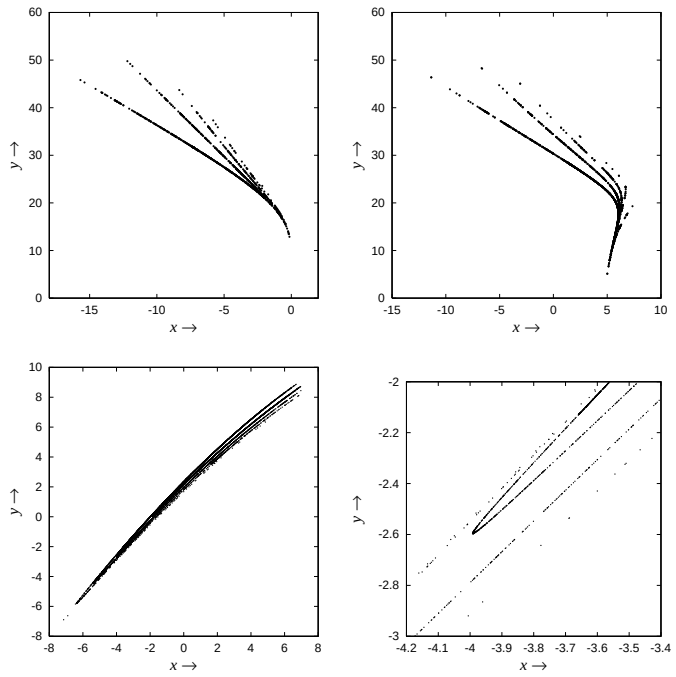

Figure 14: Poincaré map. (a): $y = 0$; (b)$y = \sqrt{(2c - a)b}$; (c): $z = 2c - a$, $y > x$; (d): an enlargement of (c).

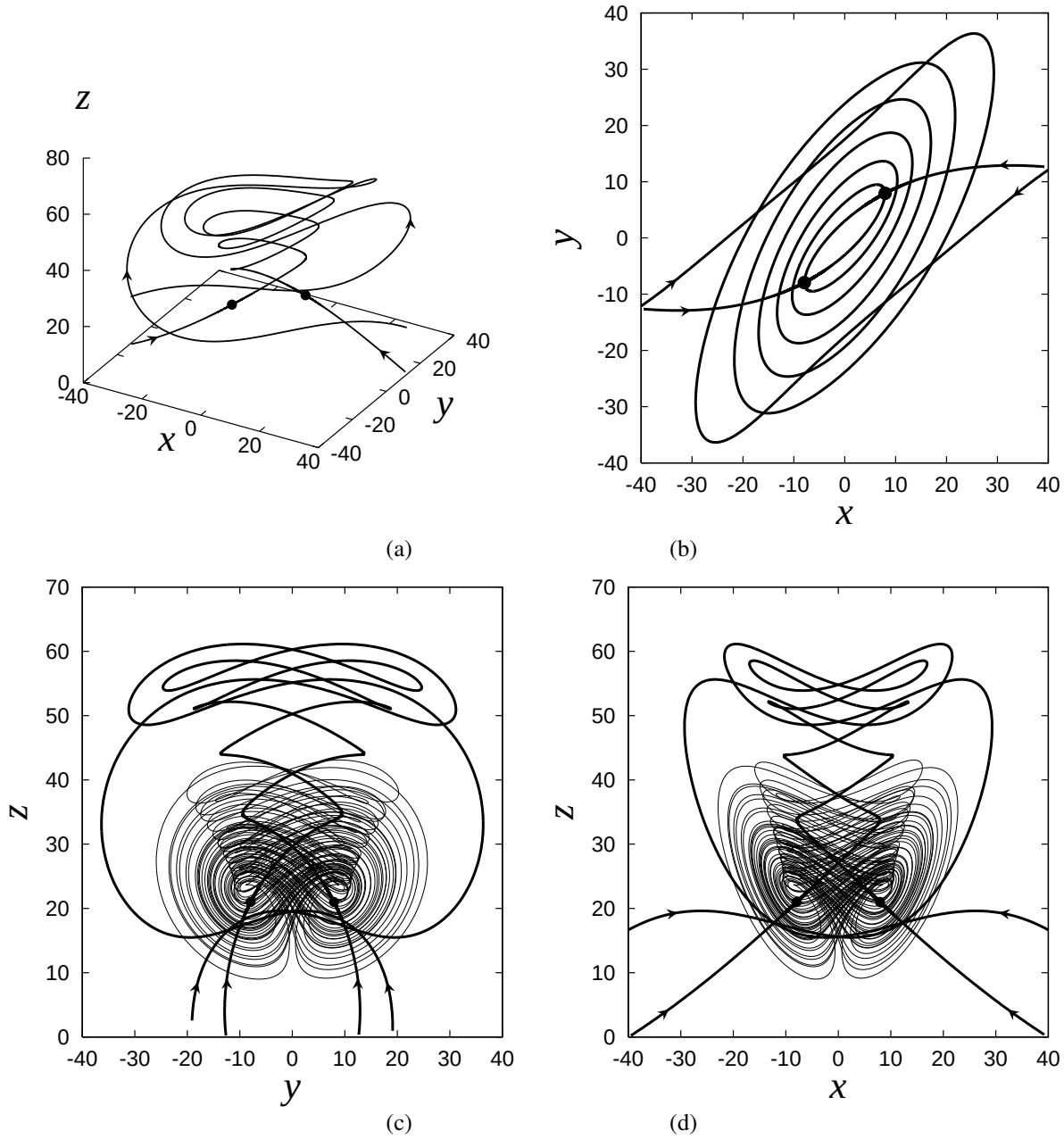

Figure 15: Stable manifolds of C^+ and C^-. $a = 35$, $b = 3$, $c = 28$. The chaotic attractor is superimposed in (c) and (d).

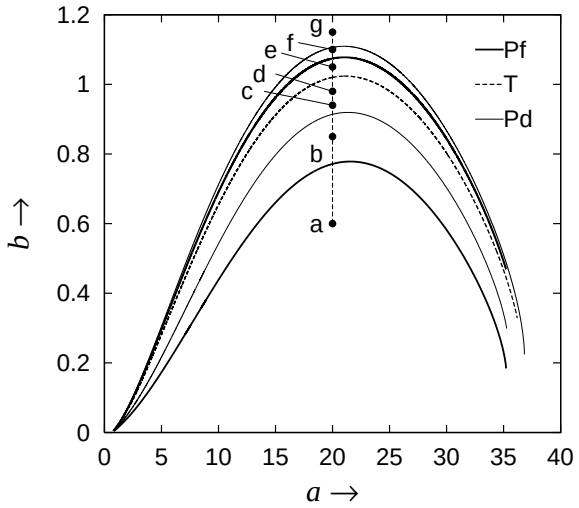

Figure 16: Bifurcation diagram of the Lorenz system (18). $c = 28$.

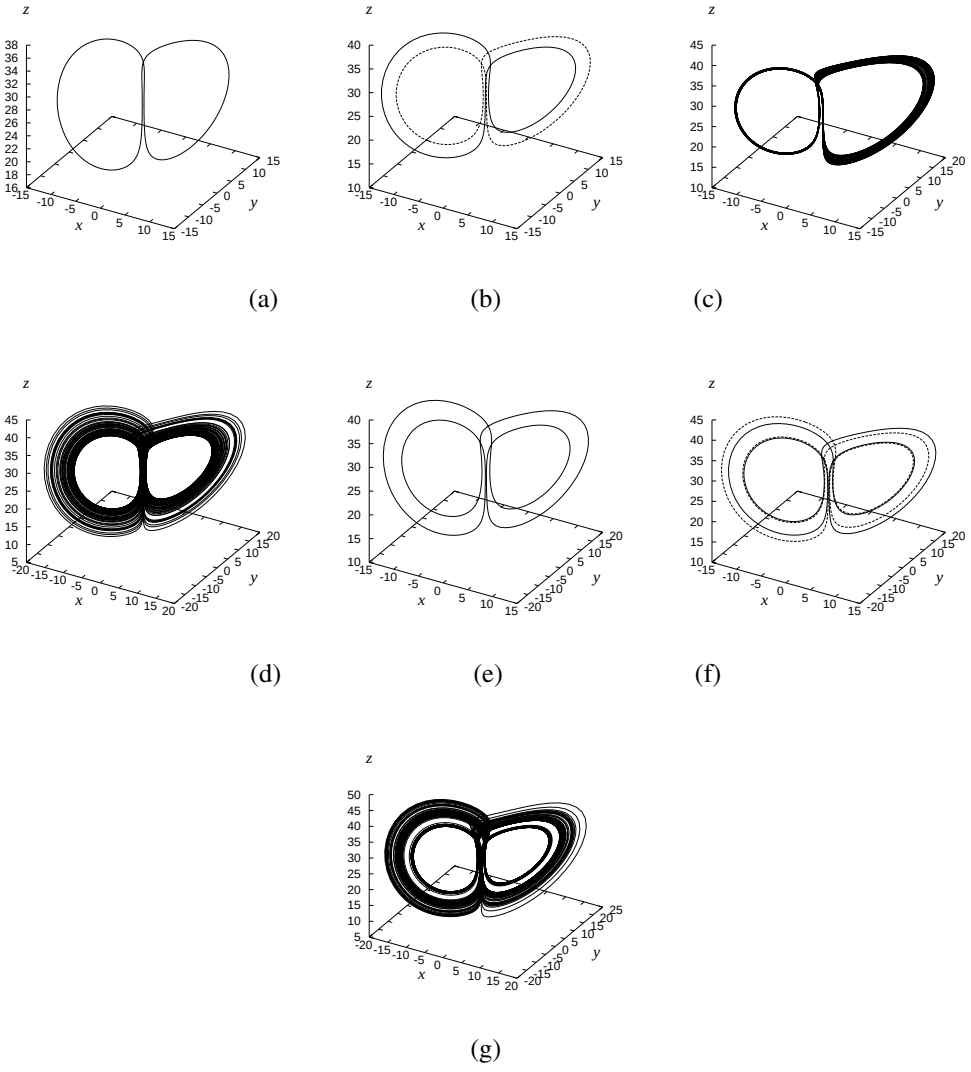

Figure 17: Phase portrait of Eq. (18). $c = 28$. (a) $b = 0.6$, (b) $b = 0.85$, (c) $b = 0.94$, (d) $b = 0.98$, (e) $b = 1.05$, (f) $b = 1.1$, (g) $b = 1.15$.

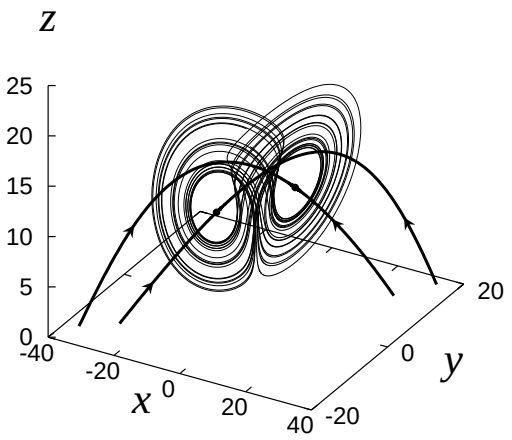

Figure 18: Stable manifolds of C^+ and C^-. $a = 45$, $b = 2.8$, $c = 28$.